



Bates, S., Hendry, K., Pryer, H., Kinsley, C. W., Pyle, K., Woodward, E. M. S., & Horner, T. J. (2017). Barium isotopes reveal role of ocean circulation on barium cycling in the Atlantic. *Geochimica et Cosmochimica Acta*, 204, 286-299. <https://doi.org/10.1016/j.gca.2017.01.043>

Peer reviewed version

License (if available):  
Unspecified

Link to published version (if available):  
[10.1016/j.gca.2017.01.043](https://doi.org/10.1016/j.gca.2017.01.043)

[Link to publication record in Explore Bristol Research](#)  
PDF-document

This is the accepted author manuscript (AAM). The final published version (version of record) is available online via Elsevier at <https://doi.org/10.1016/j.gca.2017.01.043> . Please refer to any applicable terms of use of the publisher.

## University of Bristol - Explore Bristol Research

### General rights

This document is made available in accordance with publisher policies. Please cite only the published version using the reference above. Full terms of use are available:  
<http://www.bristol.ac.uk/pure/about/ebr-terms>

1 **Barium isotopes reveal role of ocean circulation on barium cycling in the Atlantic**

2

3 **Stephanie L. Bates<sup>1</sup>, Katharine R. Hendry\*<sup>1</sup>, Helena V. Pryer<sup>1,2</sup>, Christopher W. Kinsley<sup>2,3</sup>, Kimberley**  
4 **M. Pyle<sup>1</sup>, E. Malcolm S. Woodward<sup>4</sup>, and Tristan J. Horner<sup>2,5</sup>**

5 <sup>1</sup> School of Earth Sciences, University of Bristol, Wills Memorial Building, Queen's Road, Bristol, BS8  
6 1RJ, UK; \*corresponding author [K.Hendry@bristol.ac.uk](mailto:K.Hendry@bristol.ac.uk)

7 <sup>2</sup> NIRVANA Laboratories, Woods Hole Oceanographic Institution, Woods Hole, MA 02543, USA

8 <sup>3</sup> Department of Earth, Atmospheric and Planetary Sciences, Massachusetts Institute of Technology,  
9 Cambridge, MA 02139, USA

10 <sup>4</sup> Plymouth Marine Laboratory, Prospect Place, The Hoe, Plymouth PL1 3DH, UK

11 <sup>5</sup> Department of Marine Chemistry and Geochemistry, Woods Hole Oceanographic Institution,  
12 Woods Hole Road, Woods Hole, MA 02543, USA

13

14 **Abstract**

15 We diagnose the relative influences of local-scale biogeochemical cycling and regional-scale ocean  
16 circulation on Atlantic barium cycling by analyzing four new depth profiles of dissolved Ba  
17 concentrations and isotope compositions from the South and tropical North Atlantic. These new  
18 profiles exhibit systematic vertical, zonal, and meridional variations that reflect the influence of both  
19 local-scale barite cycling and large-scale ocean circulation. Previously reported epipelagic decoupling  
20 of Ba and Si in the tropics is also found to be associated with significant Ba isotope heterogeneity.  
21 We contend that this decoupling originates from the depth segregation of opal & barite formation  
22 but is exacerbated by weak vertical mixing, as in the tropics. Zonal influence from isotopically-  
23 'heavy' water masses in the western North Atlantic evidence the advective inflow of Ba-depleted  
24 Upper Labrador Sea Water, which is not seen in the eastern basin or the South Atlantic. Meridional  
25 variations in Atlantic Ba isotope systematics below 2,000 m appear entirely controlled by  
26 conservative mixing. Using an inverse isotopic mixing model, we calculate the Ba isotope  
27 composition of the Ba-poor northern end member as +0.45 ‰ and the Ba-rich southern end  
28 member +0.26 ‰, relative to NIST SRM 3104a. The near-conservative behaviour of Ba in the deep  
29 ocean indicates that Ba isotopes may serve as an independent tracer of the provenance of advected  
30 water masses in the Atlantic Ocean. The clearly resolved Ba-isotope signatures of northern- and  
31 southern-sourced waters may also prove useful in paleoceanographic studies, should appropriate  
32 sedimentary archives be identified. Overall, our results offer new insights into the controls on Ba  
33 cycling in seawater and thus the mechanisms that underpin the utility of Ba-based proxies in  
34 paleoceanography.

35  
36  
37  
38  
39  
40  
41  
42  
43  
44  
45  
46  
47  
48  
49  
50  
51  
52  
53  
54  
55  
56  
57  
58  
59  
60  
61  
62  
63  
64  
65  
66  
67

## 1. Introduction

The oceanic biological pump effectively strips nutrients and carbon out of the surface into deep waters (Riebesell et al., 2007). Silicic acid ( $\text{Si(OH)}_4$ ) is a crucial nutrient for organisms such as diatoms, which are responsible for exporting half of the organic matter that becomes sequestered in marine sediments (Nelson et al., 1995; Tréguer and De la Rocha, 2013).  $\text{Si(OH)}_4$  and other nutrients in low-latitude regions are sourced from thermocline waters, which are fed largely from high-latitude preformed nutrients, in addition to the spatially variable fraction sourced from remineralisation (Sarmiento et al., 2004). Quantifying past changes in the supply of nutrients, such as  $\text{Si(OH)}_4$ , is key to understanding past variations in the biological pump, carbon cycling and the global climate. Barium (Ba) can help us understand such processes, because there are strong, global links between Ba and other key elements in both dissolved and particulate phases: dissolved Ba shows links with  $\text{Si(OH)}_4$  both vertically and spatially, and particulate Ba varies spatially with particulate organic carbon (POC) (Bishop, 1989).

The associations between dissolved Ba and  $\text{Si(OH)}_4$ , and particulate Ba and POC export, have led to the development of a number of Ba-based palaeoceanographic proxies. For example, Ba incorporation into carbonates (denoted by Ba/Ca) is used as a proxy for seawater dissolved Ba concentration (denoted by [Ba]) and by extension any tracer with a similarly-shaped dissolved profile e.g. alkalinity,  $\text{Si(OH)}_4$ , and DIC (Hall and Chan, 2004a, b; Lea and Boyle, 1989, 1991). Another approach builds on evidence that particulate ‘excess Ba’ (denoted as  $\text{Ba}_{\text{xs}}$ ; i.e. any Ba present in particles that is unsupported by lithogenic material) correlates with POC fluxes in suspended particulates (Dehairs et al., 1991), sediment traps (Cardinal et al., 2005), and POC export (Eagle et al., 2003). These observations instigated the interpretation of  $\text{Ba}_{\text{xs}}$  from marine sediment cores as a proxy for POC fluxes, allowing the reconstruction of export production and the biological pump through time (Dymond et al., 1992; Eagle et al., 2003; Gingele and Dahmke, 1994; Nurnberg et al., 1997).  $\text{Ba}_{\text{xs}}$  that reaches the sediments with sequestered organic matter is assumed to be well-preserved due to the saturation of porewaters with respect to barite (Paytan and Kastner, 1996). However, quantification of nutrient cycling and export production from sedimentary Ba-based archives is still hampered by the lack of a complete mechanistic understanding of barite preservation and the linkages between  $\text{Ba}_{\text{xs}}$ , nutrients, POC export, and their spatially variable relationships (Hernandez-Sanchez et al., 2011).

68           Given the strong empirical correlations between particulate Ba and POC export fluxes, and  
69 dissolved Si and Ba concentrations in seawater, then what is known about the mechanistic controls  
70 on Ba distributions? Several explanations have been proposed for the nutrient-like behaviour of Ba  
71 in seawater, though there is now considerable laboratory (Ganeshram et al., 2003; González-Munoz  
72 et al., 2003), field (Collier and Edmond, 1984; Dehairs et al., 1980), morphological (Bertram and  
73 Cowen, 1997), geochemical (Griffith and Paytan, 2012), and thermodynamic (Monnin et al., 1999)  
74 evidence to suggest that the formation of discrete, micron-sized barite ( $\text{BaSO}_4$ ) crystals in the water  
75 column is a biological or biologically-mediated process, and that  $\text{BaSO}_4$  is the major vector of  
76 particulate Ba in the modern water column. However, these observations do not address the  
77 mechanisms behind the similar depth profiles of [Ba] and  $\text{Si(OH)}_4$ , which have been proposed to  
78 relate to the similar remineralization depths of their respective carrier phases ( $\text{BaSO}_4$  and opal,  
79 respectively; e.g. Broecker and Peng, 1982), or perhaps due to the lateral advection and circulation  
80 of conservative nutrients (Horner et al., 2015), with a Ba/Si ratio set by surface processes in the high-  
81 latitudes where the water masses form (Sarmiento et al., 2004). Although advected and organic  
82 matter-derived nutrients are traditionally labelled ‘preformed’ and ‘regenerated’ respectively, here  
83 we instead use the terms ‘conservative’ and ‘non-conservative’ to refer to these two components of  
84 Ba distributions. This choice of terminology is intended to highlight that not only organic matter  
85 remineralisation but also other processes, such as barite cycling, have potentially important effects  
86 on ‘regenerated’ Ba, and because there is no ‘Redfieldian’ (i.e. fixed) stoichiometry between  
87 dissolved Ba and organic matter that that enables back-calculation of preformed Ba from P or  $\text{O}_2$   
88 (e.g. Collier and Edmond, 1984).

89           Barium stable isotope analysis provides a new and powerful approach for investigating Ba  
90 cycling in seawater (Cao et al., 2016; Horner et al., 2015), as isotopic tracers are sensitive to ocean  
91 mixing *and* biogeochemistry: the precipitation of barite—a non-conservative process—preferentially  
92 incorporates the lighter isotopes of Ba (Böttcher et al., 2012; Miyazaki et al., 2014; Nan et al., 2015;  
93 Von Allmen et al., 2010), rendering residual waters depleted in Ba and isotopically ‘heavier’ than  
94 before precipitation occurred. In contrast, ocean mixing—a conservative process—does not  
95 fractionate isotopic distributions; resultant concentration and isotopic patterns follow predictable  
96 isotopic mixing schemes (Hoefs, 2015). Hence, the information provided by seawater Ba isotopes,  
97 when used in combination with [Ba], can shed light on whether variations in [Ba] are driven by  
98 conservative mixing of different water masses or by non-conservative barite cycling, including both  
99 the formation and dissolution of particles via lateral and vertical transport. Only a few data exist for  
100 the isotopic composition of barium in seawater (Cao et al., 2016; Horner et al., 2015), and they show  
101 that isotopic variations reflect a combination of ocean circulation and barite cycling, with the latter

102 evidenced by the presence of Ba-depleted, isotopically heavy subsurface waters. A South Atlantic  
103 profile showed that, in the deep ocean, Ba isotopic values are largely a function of the circulation of  
104 major water masses falling on a conservative mixing line between Antarctic Intermediate Water  
105 (AAIW), North Atlantic Deep Water (NADW), and Antarctic Bottom Water (AABW), with end-  
106 members likely determined by barite cycling in high latitude surface waters (Horner et al., 2015). A  
107 Ba isotope profile from the East China Sea illustrated that freshwater input can also influence the Ba  
108 isotopic composition of near-surface seawater, with Ba cycling in the upper water column  
109 dominated by removal of lighter isotopes onto particles (Cao et al., 2016).

110 The main aim of this study is to investigate water column Ba concentrations and isotopic  
111 distributions both vertically, zonally, and meridionally within the Atlantic. We use these data to  
112 examine the impact of BaSO<sub>4</sub> precipitation and dissolution on Atlantic Ba cycling, and quantify the  
113 relative mixing proportions of northern- and southern-sourced water masses using new seawater  
114 depth profiles from both the eastern and western basins. Firstly, we use the isotopic composition of  
115 dissolved Ba in seawater to investigate subtle near-surface variations in its concentration, and its  
116 decoupling from Si, in the tropical North Atlantic. Secondly, we use seawater Ba isotopes to trace the  
117 proportion of deep ocean variation that is attributable to lateral advection (conservative mixing) vs.  
118 barite cycling (and other non-conservative vertical processes) in these tropical locations. Lastly, we  
119 compare our new tropical North Atlantic data with our profiles from the South Atlantic in order to  
120 investigate the extent to which basin-scale Ba distributions are driven by mixing, as opposed to  
121 barite cycling.

122

## 123 **2. Methods and materials**

124

### 125 *2.1. Oceanographic setting*

126 We present data from the South and tropical North Atlantic, which are both influenced by  
127 similar water masses at different stages of the Atlantic meridional overturning circulation (Talley,  
128 2013). In the South Atlantic, the water column is composed of southern-sourced AABW (below  
129 3500m), southward flowing NADW (2000-3500m), Upper Circumpolar Deep Water (core at c.  
130 1500m), AAIW (core at c. 600m) and a mixture of Subantarctic Surface Water (SASW) and  
131 Subtropical Surface Water (STSW). In the Equatorial Atlantic, AABW occurs below ~4000m, AAIW at  
132 c. 1000m (mixed with Mediterranean Water), NADW below ~1500-2000m, and tropical mode and  
133 surface waters subduct to form the thermocline (Talley et al., 2011).

134

### 135 *2.2. Sample collection*

136 Seawater collection and processing procedures for samples from the South Atlantic  
 137 (D357/GA10E; Oct-Nov 2010) are discussed in Horner et al. (2015). Samples from the tropical North  
 138 Atlantic (JC094; Oct-Nov 2013) were collected using Niskin bottles attached to a CTD rosette system,  
 139 filtered cleanly through a 0.2 micron Acropak filter (Pall Life Sciences) and samples for Ba analysis  
 140 were acidified (0.1% v/v; pH  $\approx$  2.0) the same day using concentrated hydrochloric acid (HCl Romil  
 141 UpA). Samples were stored in a cool container (+4°C) for transport back to the UK. Sampling stations  
 142 are shown in Table 1.

143 Temperature, conductivity, and fluorescence were measured using a Sea-Bird (SBE) *9plus*  
 144 with a Chelsea Technology Group (CTG) Aquatracka MKIII fluorimeter, and data were post-processed  
 145 using SBE Data Processing (V7.20g) software. Salinity was calculated from conductivity, and  
 146 calibrated on board using bottle samples measured using a GuildLine Autosol salinometer, with  
 147 Autosol software (2009). Dissolved Oxygen was measured using an SBE 43 dissolved oxygen sensor  
 148 mounted on the CTD, and calibrated using bottle measurements, which were carried out on board  
 149 by the Winkler titration method using a  $\Omega$ -Metrohm 848 Titrino plus unit, with potentiometric end  
 150 point detection (Carritt and Carpenete, 1966; Robinson, 2014).

151

Cruise	CTD number	Station	Latitude	Longitude	Water depth (m)
JC094	CTD002 (CTD2)	002	9° 17.1'N	21° 38.0'W	4524
JC094	CTD005 (CTD5)	039	10° 51.8'N	44° 29.5'W	5161
JC094	CTD006 (CTD6)	044	15° 16.2'N	48° 15.6'W	4183
D357	CTD025 <sup>a</sup>	6	39° 59.4'S	0° 55.2'E	4927
D357	CTD013	3	36° 27.6'S	13° 23.4'E	4894

152 *Table 1: Locations of CTD profiles used in this study. <sup>a</sup> From Horner et al., 2015.*

153

154 Additional unfiltered samples were collected for nutrient analysis and frozen at -20°C for  
 155 transport back to the UK. Nitrate+Nitrite, Nitrite, Silicate, Phosphate and Ammonium were analysed  
 156 using a Bran and Luebbe 5 channel segmented flow autoanalyser (Plymouth Marine Laboratories,  
 157 UK), and with high resolution colorimeters (Brewer and Riley, 1965; Grasshoff et al., 1999; Kirkwood,  
 158 1989; Zhang and Chi, 2002). Samples were defrosted back on land over 48 hours at room  
 159 temperature, in the dark, before being analysed alongside a certified nutrient reference material  
 160 produced by KANSO Technos, Japan. The KANSO Technos reference materials are analysed on a daily  
 161 basis as part of the regular analytical protocols, and have allowed the results stated here to have an  
 162 accuracy of 2% or better when compared to these reference concentrations. By adopting analytical

163 methods and techniques according to GO-SHIP protocols, improvements and checks are made to  
164 ensure and check the analytical accuracy of the analyses of the nutrients. Precision is again at or  
165 better than 2% when this is determined along with the regular sample analysis. The standard used  
166 are all high quality materials, and will always be analysed to have the highest standard as greater  
167 than the highest concentrations of the samples, and standards will be ensured as being a linear slope  
168 to allow full confidence of the reported concentrations of samples.

169

### 170 *2.3. Barium isotope analysis*

171 Seawater Ba concentrations and isotopic compositions were measured at the NIRVANA Lab  
172 at Woods Hole Oceanographic Institution (WHOI) using a method similar to that of Horner et al.  
173 (2015), which consists of double spiking, co-precipitation, and ion-exchange chromatography  
174 followed by Ba isotope analysis via MC-ICP-MS (multiple-collector inductively-coupled plasma mass  
175 spectrometry). A new double spike composed of roughly equal proportions of  $^{135}\text{Ba}$  and  $^{136}\text{Ba}$  was  
176 used instead of the  $^{135}\text{Ba}$ - $^{137}\text{Ba}$  double spike previously described by Horner et al. (2015; see  
177 Supplement for spike composition). The new choice of spike combination was optimized to minimize  
178 the impact of interferences from Xe – present as a trace impurity in the Ar carrier gas – found on  $m/z$   
179 136 (Xe, Ba, Ce) during MC-ICP-MS analysis.

180 Barium concentrations were estimated from dissolved [Si] values and an appropriate  
181 amount of  $^{135}\text{Ba}$ - $^{136}\text{Ba}$  double spike was added to 5 ml of seawater to achieve roughly equal  
182 proportions of spike- and sample-derived Ba in the spike—sample mixture. In accordance with  
183 GEOTRACES protocols (Cutter et al., 2010), additional ultra-pure HCl was added to the tropical North  
184 Atlantic samples at WHOI to achieve a final HCl concentration of 0.024 M (pH < 2). Spike-sample  
185 mixtures were refluxed at 60 °C for 24 hours, allowed to cool to room temperature, then co-  
186 precipitated through the addition of 350  $\mu\text{l}$  of 1 M  $\text{Na}_2\text{CO}_3$  solution in 50  $\mu\text{l}$  increments (Foster et al.,  
187 2004). After centrifugation and decantation of residual seawater, precipitates were dissolved in ~2  
188 M HCl, dried, and resuspended in 250  $\mu\text{l}$  of 2.3 M HCl for ion-exchange chromatography. Purification  
189 of Ba was achieved by passing samples twice through 500  $\mu\text{l}$  of AG 50W-X8 (200–400 mesh) cation  
190 exchange resin that was precleaned and conditioned with 6 M and 2.3 M HCl, respectively. Non-Ba  
191 matrix elements were eluted with 2.3 M HCl, followed by Ba elution using 2 M nitric acid ( $\text{HNO}_3$ ).  
192 Purified samples were subsequently dried, to oxidize any resin-derived organic material that may  
193 have co-eluted with Ba – dried again, and finally re-dissolved in 2 %  $\text{HNO}_3$  for mass spectrometric  
194 analysis.

195 Samples were analysed for barium isotope compositions at the WHOI Plasma Facility using a  
196 Thermo Neptune MC-ICP-MS operated in low-resolution mode, fitted with 'Regular'- and 'X'-type

197 sampler and skimmer Ni interface cones, respectively. Samples were aspirated at ~120  $\mu\text{l}/\text{min}$  using  
 198 an Elemental Scientific PFA  $\mu\text{Flow}$  nebulizer, via a CETAC Aridus II desolvator, and admixed with 3–5  
 199 ml/min  $\text{N}_2$  gas to reduce  $\text{BaO}^+$  formation  $\leq 0.1\%$  during Ba ionization (Miyazaki et al., 2014).  
 200 Baseline-corrected ion beams corresponding to  $m/z = 131$  (Xe), 135 (Ba), 136 (Xe, Ba, Ce), 137 (Ba),  
 201 138 (Ba, La, Ce), 139 (La), and 140 (Ce) were measured simultaneously by  $40 \times 4.194$  s integrations at  
 202 sample-derived Ba concentrations of around 20 ng/ml;  $\text{Ba}^+$  transmission efficiencies were generally  
 203  $\geq 1\%$ . Barium isotope compositions were calculated in MATLAB using the three-dimensional  
 204 geometric interpretation of the double spike problem (Siebert et al., 2001). In this interpretation,  
 205 the  $x$ -,  $y$ -, and  $z$ - axes are defined by  $^{138}\text{Ba}/^{135}\text{Ba}$ ,  $^{137}\text{Ba}/^{135}\text{Ba}$ , and  $^{136}\text{Ba}/^{135}\text{Ba}$ , and interference  
 206 corrections for Xe, Ce, and La were performed via the nested iterative approach described in Horner  
 207 et al. (2015). Sample-derived Ba concentrations are calculated based on the instrumental mass bias-  
 208 corrected  $^{138}\text{Ba}/^{135}\text{Ba}$  ratio (noting that most  $^{135}\text{Ba}$  is spike-derived) and *a priori* knowledge of the  
 209 spike added to each sample. Isotopic compositions are reported in the  $\delta$ -notation relative to  
 210 National Institute of Standards and Technology (NIST) Standard Reference Material 3104a (Ba):

$$211 \quad \delta^{138/134}\text{Ba}_{\text{NIST}} = \left\{ \frac{\left( \frac{^{138}\text{Ba}}{^{134}\text{Ba}} \right)_{\text{sample}}}{\left( \frac{^{138}\text{Ba}}{^{134}\text{Ba}} \right)_{\text{NISTSRM 3104a}}} - 1 \right\} \times 1000 \quad (1)$$

212 Isotopic uncertainties are reported as the larger of either the long-term  $2 \times \text{SD}$  (Standard Deviation)  
 213 uncertainty on sample unknowns ( $\pm 0.03\%$ ,  $n = 8$ ) or the pooled internal  $2 \times \text{SE}$  (Standard Error) of  
 214 repeat sample measurements (median number of replicate analyses = 4.), as described in Horner et  
 215 al. (2015).

216 Blanks were monitored by passing aliquots containing  $\sim 1$  ng of Ba double spike through the  
 217 procedures described above and treating as sample unknowns. The mean analytical blank (from  
 218 reagents and ion-exchange chemistry) was measured as  $11 \pm 8$  pg (mean  $\pm 1$  SD;  $n = 4$ ) and the  
 219 procedural blank (co-precipitation plus analytical blank) was determined as  $726 \pm 124$  pg (mean  $\pm 1$   
 220 SD;  $n = 6$ ). All seawater Ba concentration data were procedural-blank corrected but Ba isotope data  
 221 were not as the small proportion of blank-derived Ba in seawater samples was deemed unlikely to  
 222 alter Ba isotope compositions outside of long-term uncertainty ( $\pm 0.03\%$ ; Horner et al., 2015).  
 223 Additional details regarding the reporting of uncertainty are presented in the Supplementary  
 224 Information.

225  
 226

### 227 3. Results



228

### 229 3.1. Temperature, salinity, oxygen and nutrient profiles

230 The potential temperature and salinity measurements show typical profiles for the South  
231 Atlantic and tropical Atlantic sites, with marked latitudinal differences above 3000m water depth.  
232 Near-surface and subsurface temperatures are over 15°C warmer in the tropics than the South  
233 Atlantic, and significantly more saline (Fig. 2 A, B). The oxygen profiles from the tropical Atlantic sites  
234 show a pronounced minimum centred on approximately 500m water depth, absent from the South  
235 Atlantic sites, and higher oxygen levels at depth than at 40°S (Fig. 2C).

236 Nutrients showed expected concentration profiles (Fig. 2 D, F), with low concentrations at  
237 the surface as a result of biological uptake, and higher values at depth as a result of lateral transport  
238 of conservative nutrients and regeneration. Regenerated nutrients are represented by  $N^*$  (not  
239 plotted;  $N^* = NO_3^- - 16PO_4$ ) and  $Si^*$  (Fig. 2E) where  $Si^* = [Si(OH)_4] - [NO_3] + dN^*$ , where the  
240 denitrification correction  $d = 1$  for  $N^* < -3$   $\mu M$  ( $d = 0$  otherwise) (Gruber and Sarmiento, 1997;  
241 Sarmiento et al., 2004). No denitrification correction was required for the Equatorial Atlantic  
242 samples.  $Si^*$  is only conserved when remineralisation (or uptake) processes release (or take up)  
243  $Si(OH)_4$  and  $NO_3$  in a 1:1 ratio, which is not the case in regions of the Southern Ocean where AAIW  
244 and mode waters are formed as a result of strong nutrient uptake by iron limited diatoms  
245 ( $Si(OH)_4:NO_3$  uptake ratio  $\sim 4:1$ ; Brzezinski et al., 2002; Sarmiento et al., 2004). Hence,  $Si^*$  is a  
246 powerful tracer of Southern Ocean intermediate depth waters, and can be used to pinpoint AAIW at  
247  $\sim 1000m$  depth in our North Atlantic depth profiles (Fig. 2).

248

### 249 3.2. Barium and barium isotopes

250 Water column Ba concentrations from our new seawater profiles show the now well-  
251 established vertical fractionation of [Ba], with lower values in surface waters ( $\sim 40$  nM) and higher  
252 values at depth ( $\sim 80$  nM for the tropical Atlantic profiles,  $\sim 100$  nM for the new Southern Atlantic  
253 profile; Fig. 3; Supplementary information). [Ba] increases down the water column from  $\sim 1500m$  to  
254  $5000m$  in all the new profiles; the tropical Atlantic profiles show a slight increase of  $< 5$  nM at  
255  $\sim 1000m$ , before declining again towards the subsurface. The shallower samples of the profiles,  
256 above  $\sim 50m$ , show that [Ba] increases slightly by  $\sim 5$  nM towards the surface. The  $\delta^{138}Ba$  values  
257 generally mirror [Ba], becoming progressively lighter as [Ba] increases, in good agreement with the  
258 previously published South Atlantic  $\delta^{138}Ba$  profile (Horner et al., 2015). The tropical Atlantic  $\delta^{138}Ba$   
259 data differ from the published South Atlantic profile in two respects. Firstly, surface  $\delta^{138}Ba$  profiles  
260 show heavier values at approximately  $200m$  ( $\sim +0.6$  ‰), followed by a decline of  $\sim 0.1$  ‰ towards  
261 lighter values at the surface in the tropical Atlantic samples only (Fig. 3). Secondly, there is a

262 divergence in both [Ba] and  $\delta^{138}\text{Ba}$  between the tropical Northwest Atlantic and Northeast Atlantic  
263 samples in the mid-depths, centred around a core at approximately 1500m.

264

## 265 **4. Discussion**

266

### 267 *4.1. Ba\* (barium star)*

268 These new [Ba] and  $\delta^{138}\text{Ba}$  profiles, especially when assessed in the context of a previously  
269 published South Atlantic depth profile (Horner et al., 2015), provide a new insight into the relative  
270 roles of different processes that affect Atlantic Ba cycling: conservative versus non-conservative  
271 barium, the depth ranges of organic matter and barite remineralisation, and water mass mixing.  
272 These processes can be further quantified by combining measurements of  $\delta^{138}\text{Ba}$  with Ba\*, which is  
273 defined as the difference between *in situ* and predicted [Ba]:

$$274 \text{Ba}^* = [\text{Ba}]_{in\ situ} - 0.6296(\pm 0.0022) * [\text{Si}(\text{OH})_4]_{in\ situ} - 38.63(\pm 0.07) \quad (2)$$

275 This formulation of Ba\* is based on a York Regression of 1,505 globally-distributed [Ba]–[Si]  
276 measurements from the GEOSECS expeditions (Geochemical Ocean Sections; e.g. Craig and Turekian,  
277 1980), and differs slightly from the formulation used by Horner et al. (2015), which was based only  
278 on GEOTRACES-era co-located [Ba]–[Si] measurements from the South Atlantic. Regardless, the  
279 absolute values of Ba\* are essentially arbitrary – the utility of Ba\* is derived from the shape of the  
280 depth profiles. Vertical profiles of Ba\* that vary with depth arise from subtle variations in the  
281 integrated histories of Ba and Si cycling that relate to differences in the ventilation of preformed  
282 water masses, and uptake and remineralisation processes of the two elements: barite precipitation  
283 and dissolution affects the cycling of Ba but not Si, whereas biological opal formation and dissolution  
284 impacts the cycling of Si but not Ba. For example, the water column profiles of Ba\* show more  
285 negative values in the mesopelagic zone, in both the North and South Atlantic, which trending  
286 towards more positive values below approximately 2000m before become more negative again  
287 below 3000m (Figure 4). The shape of these profiles arise as a result of sampling different water  
288 masses with different physiochemical properties, locations of origin and ventilation ages.

289

### 290 *4.2. Surface and near-surface cycling of barium*

291 The depth profiles of Ba\*, and  $\delta^{138}\text{Ba}$ -Ba\* plots (Figs. 3, 4), of our new data indicate that  
292 there are marked latitudinal differences in sub-surface processes that influence the barium cycle in  
293 the Atlantic, with a gradient in Ba\* between latitudes and more heterogeneous  $\delta^{138}\text{Ba}$  near surface  
294 values in the tropics compared to the South Atlantic. Of particular interest are the heavy near-  
295 surface isotopic values that trend lighter towards the surface in the North Atlantic, compared to the

296 relatively homogeneous near-surface waters of the South Atlantic at 40°S (Fig. 4; Fig. 5; Horner et al.,  
297 2015)—this could potentially relate to differences in biological production (Tilstone et al., 2015), or  
298 to differences in the physical structure of the mesopelagic layer between the N and S Atlantic.

299 The heavy Ba-isotopic values in the sub-surface (relative to deeper waters) throughout the  
300 Atlantic are likely a result of barite formation, which preferentially incorporates isotopically light Ba  
301 (Von Allmen et al., 2010), thus rendering residual seawater isotopically heavier and depleted in Ba.  
302 We can calculate an apparent fractionation factor ( $\epsilon'$ ) for barite formation in the mesopelagic and  
303 near-surface layers, by solving the following equations using iterative linear regression (Marquardt-  
304 Levenberg algorithm), which assume a closed or open fractionation respectively:

$$305 \quad \delta^{138}\text{Ba} = \epsilon' \ln([\text{Ba}]) + c$$

$$306 \quad \delta^{138}\text{Ba} = \epsilon' ([\text{Ba}]/[\text{Ba}]_0) + c \quad (3)$$

307 Where  $[\text{Ba}]_0$  is the barium concentration of the water supplying the mesopelagic layer (after  
308 Varela et al., 2004), and  $c$  is the intercept (for more details, see the Supplementary Information).  
309 Using this method, the apparent fractionation factor is calculated to be  $-0.34 \pm 0.06\text{‰}$  (closed) or -  
310  $0.45 \pm 0.08\text{‰}$  (open) for the North Atlantic, and  $-0.28 \pm 0.03\text{‰}$  (closed) or  $-0.39 \pm 0.04\text{‰}$  (open) for  
311 the South Atlantic (uncertainties represent the standard error). Whilst these values agree well with  
312 previous estimates of Ba isotopic fractionation during barite formation in the laboratory (Von Allmen  
313 et al., 2010), these estimates are likely to underestimate the true fractionation factor as the simple  
314 assumptions of the fractionation models are often violated in complex oceanic settings. Moreover,  
315 the study of Cao et al (2016), identified that the  $\Delta^{138}\text{Ba}$  offset between particles and seawater was  
316 significantly larger than estimated here using Rayleigh-type fractionation models.

317 Barite formation is likely associated with organic matter decomposition by heterotrophic  
318 bacteria, and high particulate  $\text{Ba}_{\text{xs}}$  has been seen to be associated with organic matter  
319 remineralisation and oxygen consumption at the top of the mesopelagic layer (Cardinal et al., 2005;  
320 Dehairs et al., 2008; Jacquet et al., 2007; Jacquet et al., 2008). The oxygen minimum (which mirrors  
321 the apparent oxygen utilization and is more pronounced in the tropics) and chlorophyll maxima  
322 occur at different depths in the two locations (Fig. 5), potentially contributing to differences in sub-  
323 surface  $\text{Ba}^*$  and  $\delta^{138}\text{Ba}$  profiles. Biological net community production at 40°S is markedly higher than  
324 in the Equatorial Atlantic (Tilstone et al., 2015), and variations in organic matter availability, and  
325 hence barite formation, could explain the sub-surface latitudinal differences observed here.  
326 However, mass balance considerations suggest that, whilst it is important for particulate barite  
327 formation, Ba directly associated with organic matter is likely to be unimportant in terms of setting  
328 the depth profile of Ba and Ba isotopes in the dissolved phase (Horner et al., 2015). Thus, neither the  
329 amount of nor depth of organic matter degradation (and so barite formation) can account for the

330 trend towards lighter Ba-isotopic signatures towards the surface in the tropics, a feature that is  
331 absent from the South Atlantic profiles.

332 We suggest that the differences in the North and South Atlantic sub-surface water column  
333 profiles of Ba\* and  $\delta^{138}\text{Ba}$  are as a result of the interplay between the physical structure of the upper  
334 water column and the vertical segregation of BaSO<sub>4</sub> and opal precipitation. Mixed layer depths  
335 (MLD) are shallower (less than 50 m) in the tropical Atlantic compared to the South Atlantic  
336 (maximum MLD greater than 100–150 m; Fig. 1), owing to a cap of low density water in the  
337 Subtropics. Although both sampling events reported here were carried out in Oct–Nov, published  
338 MLD climatologies indicate that these MLDs are likely to persist for the majority of the year (Kara et  
339 al., 2003). Regardless, if the MLD were to penetrate to the depths of barite formation, typically  
340 below 150 m (e.g. Dehairs et al., 2008; Jacquet et al., 2008), or able to entrain deeper waters that  
341 have experienced higher degrees of Ba removal into barite, the upper water column would be  
342 uniform for [Ba] Ba\*, and  $\delta^{138}\text{Ba}$ . The relatively constant [Ba], Ba\*, and  $\delta^{138}\text{Ba}$  observed in the  
343 uppermost  $\approx$  200 m of the South Atlantic water column is thus consistent with periodic  
344 homogenization of the upper water column by vertical mixing (Figs. 1, 5).

345 In contrast, mixed layers in the tropical North Atlantic do not extend much below 50 m over  
346 an annual cycle (Fig. 1; Schmidtke et al., 2013). This range does not penetrate to the depths  
347 necessary to entrain Ba-depleted STUW (Subtropical Underwater; >200 m) or to those estimated for  
348 barite formation (>150 m). The STUW are notable as they exhibit significant decoupling of Ba and Si,  
349 first noted by Chan et al. (1977). This decoupling is clearly evident in the more negative values of Ba\*  
350 in STUW compared to surface waters, implying Ba depletion relative to Si (Fig. 5C). More negative  
351 Ba\* in STUW are also associated with  $\approx$  +0.1 ‰ increase in dissolved Ba isotope compositions  
352 relative to surface waters, consistent with the removal of isotopically light Ba into BaSO<sub>4</sub> (e.g. Von  
353 Allmen et al., 2010). Such a pattern of more negative Ba\* associated with heavier Ba isotope  
354 compositions in shallow subsurface waters is only expected if two conditions are met: both the  
355 removal of Si and Ba are vertically segregated (e.g. via opal for Si and via BaSO<sub>4</sub> for Ba) and if the  
356 segregation remains protected from homogenization via vertical mixing. As both of these conditions  
357 are satisfied in the STUW of the subtropical North Atlantic, we conclude that the interplay between  
358 physical mixing and the vertical segregation of BaSO<sub>4</sub> & opal formation must be responsible for the  
359 differences between the profiles of Ba\* and  $\delta^{138}\text{Ba}$  in the subtropical North- and South Atlantic (Fig  
360 5).

361

362

363 *4.3. Barium concentrations and isotopic variations in deep and intermediate waters*

364 As with other elements with nutrient-like behaviour, an important issue in understanding  
365 oceanic cycling surrounds the relative contribution of conservative versus non-conservative Ba – the  
366 extent to which Ba distribution reflects simple mixing of different water masses rather than *in situ*  
367 dissolution. Since Ba is not directly cycled in association with organic matter (Sternberg et al., 2005),  
368 it is not possible to ‘back calculate’ conservative Ba for a given water mass from other hydrographic  
369 parameters (e.g. using [O<sub>2</sub>] and *in situ* P; Broecker et al., 1985), thus requiring an alternative  
370 approach. A further complication arises when considering where the particles originate that are  
371 involved in dissolution processes: particles may arrive at depth from vertical sinking and some others  
372 from lateral transport. At depths below the MLD, our new profiles reveal key meridional and zonal  
373 differences that reflect the relative role of ocean circulation and barite dissolution in Ba cycling, both  
374 in deep waters ( $\geq 2000\text{m}$ ) and intermediate depths (500-2000m).

375 We investigated mixing processes by plotting our data in a mixing diagram, in which  
376 conservative mixing relationships will result in straight lines. The linear relationships shown in Fig. 6a  
377 illustrates that the tropical Atlantic Ocean  $\delta^{138}\text{Ba-1/Ba}$  systematics are consistent with conservative  
378 mixing being a major control below approximately 500 m, but also that statistically-significant  
379 differences exist between the tropical- and South Atlantic datasets. (Least squares fits to the data  
380 possess statistically different intercepts and slopes for north and south Atlantic data.) The different  
381 slopes in the mixing lines from the North and South Atlantic may reflect a subtle overprint from *in*  
382 *situ* remineralisation of BaSO<sub>4</sub> and other Ba-bearing particles. This additional input of Ba would  
383 result in Ba-depleted (and initially isotopically heavy) deep waters from the north Atlantic exhibiting  
384 roughly similar Ba-isotope compositions to Ba-replete water masses from equivalent depths in the  
385 South Atlantic, despite possessing significantly less Ba. Regardless, this effect is small as the overall  
386 north Atlantic trend is linear (Fig. 6a), indicating that conservative mixing is the dominant control on  
387 Ba systematics in both the deep north and south Atlantic. Importantly, our Ba isotope data  
388 underscore the importance of conservative mixing as an important control on Atlantic Ba cycling  
389 without the need to ratio to other biogeochemical tracers (e.g. [Si],  $\underline{I}$ , S). As we show in the next  
390 section however, we can use these additional tracers to independently constrain relative deep-water  
391 mass mixing proportions, thus enabling us to estimate the Ba-isotope compositions of the end-  
392 member northern- and southern-sourced water masses that mix in the deep Atlantic.

393

#### 394 4.3.1. Meridional overturning control of deep (>2,000 m) Ba isotope distributions

395 The linear relationships between Ba-isotope compositions and 1/[Ba] illustrates that  
396 conservative mixing accounts for essentially all of the Ba-isotope variation in the deep Atlantic.  
397 Below 2000 m, the Atlantic is dominated by the mixing of nutrient-poor (and O<sub>2</sub>-rich) northern-

398 sourced waters (collectively termed NADW) with nutrient-rich southern-sourced bottom waters  
 399 from the Weddell Sea (termed here AABW). Our data can be used to place constraints on the likely  
 400 Ba isotope compositions of these two end-member water masses by independently calculating their  
 401 relative mixing proportions. Broecker et al., 1991 suggested that the fraction of northern-sourced  
 402 waters in a given sample,  $f_n$ , can be calculated using:

$$403 \quad f_n = (1.67 - PO_4^*) / (1.67 - 0.73) \quad (4)$$

404 where  $PO_4^* = [PO_4^{3-}] + ([O_2] / 175) - 1.95$ . If we compare our Ba isotope data for samples below  
 405 2,000 m against  $f_n$  (Fig. 6b), we observe a distinct curvature that is indicative of a two-component  
 406 hyperbolic isotopic mixing trend (e.g. Mariotti et al., 1988). In order to quantify the end-members  
 407 responsible for generating the hyperbolic mixing trend, we make the simplifying assumption that  
 408 there is no influence from non-conservative biogeochemical processes below 2,000 m. Though this is  
 409 likely an oversimplification, the strong linear (mixing) relationships shown in Fig. 6a indicate that  
 410 mixing is certainly the dominant control on Ba isotope systematics in the deep Atlantic, despite  
 411 barite being below saturation at these depths. As such, we can approximate the Ba isotope  
 412 composition of a deep water mass purely in terms of mixing between northern- and southern-  
 413 sourced waters:

$$414 \quad \delta^{138/134}Ba_{in\ situ} = (f_n \times \delta^{138/134}Ba_n \times [Ba]_n) + ([1 - f_n] \times \delta^{138/134}Ba_s \times [Ba]_s) \dots \quad (5)$$

$$415 \quad \dots / (f_n \times [Ba]_n) + ([1 - f_n] \times [Ba]_s)$$

416 where  $_n$  or  $_s$  denote the northern- and southern-sourced end-members, respectively. The Ba  
 417 concentration of the northern end member was estimated to be 50 nM based on data from the  
 418 Atlantic GEOSECS Expedition (average of Labrador Sea Water, Iceland—Scotland Overflow Water,  
 419 and Denmark Strait Overflow Water; Chan et al., 1977); the southern-sourced end member was  
 420 assigned  $[Ba] = 105$  nM (based on Weddel Sea water; Hoppema et al., 2010).

421 Using the independent estimates of water mass mixing proportions from Eq. 3 and literature  
 422 values of  $[Ba]$  for the northern- and southern-sourced end members, we solved Eq. 4 for the Ba  
 423 isotope compositions of the two end-members by minimization of the data—line misfit, expressed  
 424 as the RMSD (root-mean-square deviation; Fig. 6b). This calculation was restricted to the 21 samples  
 425 from  $\geq 2,000$  m and omitted sample #W0117 (JC094), as it possessed  $f_n > 1$ . The best-fit Ba isotope  
 426 compositions for the northern- and southern-sourced water mass end members were calculated as  
 427  $\delta^{138/134}Ba_{NIST} = +0.45$  ‰ and  $+0.26$  ‰, respectively. These two end-member compositions achieve a  
 428

432 data—line RMSD of 0.03 ‰, roughly equivalent to our measurement precision of 0.03 ‰ for Ba-rich  
433 deep waters.

434 Importantly, this analysis suggests that the northern- and southern-sourced water masses  
435 that fill the deep Atlantic possess clearly resolvable Ba isotope compositions ( $\Delta^{138/134}\text{Ba}_{\text{north-south}} \approx 0.2$   
436 ‰; Fig. 6b). If this pattern is verified throughout the Atlantic basin, Ba isotope analyses of deep  
437 waters may have utility in constraining ‘ $f_n$ ’ independently of existing methods. Moreover, if  
438 sedimentary archives that faithfully record deep water Ba isotope signals can be identified, Ba  
439 isotope analyses may enable temporal reconstruction of northern- versus southern-sourced waters  
440 in the deep ocean—and thus the geometry of overturning circulation—from a single biogeochemical  
441 tracer.

442

443

444

#### 445 *4.3.2. Zonal differences: influence from Labrador Sea Water at intermediate depths (500-2000m)*

446 A zonal (east-west) difference in Atlantic Ba concentrations and  $\delta^{138}\text{Ba}$  systematics becomes  
447 clear in our new profiles centred at approximately 1500 m water depth (e.g. Fig. 3). In the western  
448 tropics (CTD005 and CTD006), dissolved Ba-isotopic compositions are  $\approx +0.1$  ‰ heavier than the  
449 values of  $\delta^{138}\text{Ba} \approx +0.4$  ‰ seen in the eastern basin (CTD002; Fig. 3). These depths correspond to  
450 the depths of recently ventilated Upper Labrador Sea Water (ULSW) as shown by hydrographic data  
451 (nutrients, dissolved oxygen, and ventilation tracers such as radiocarbon; (Chen et al., 2015; Jenkins  
452 et al., 2015) . One possible interpretation for the elevated  $\delta^{138/134}\text{Ba}$  in ULSW may relate to non-  
453 conservative processes, such as extensive barite formation or input of isotopically heavy Ba in the  
454 Labrador Sea. Input of isotopically heavy Ba into the Labrador Sea is unlikely since [Ba] is lower in  
455 ULSW compared to the equivalent water depths in the eastern tropical Atlantic (Fig. 3a). Similarly,  
456 the E—W difference in [Ba] is only  $\approx 3$  nM, and depth profiles of Ba\* from the east and western  
457 north Atlantic show similar gradients, suggesting that extensive barite formation is unlikely to be  
458 responsible for removing significant quantities of Ba from the Labrador Sea. Moreover, non-  
459 conservative processes are largely precluded by the linear mixing relationships (Fig. 6a), suggesting  
460 that the isotopically heavy Ba at the depths corresponding to ULSW are a conservative mixing  
461 feature. Thus, a simple explanation for this Ba isotope feature is that the influence from the  
462 advective inflow of ULSW is far greater in the western basin (CTD005, 006) compared to the eastern  
463 basin (CTD002), and that—since ULSW is recently ventilated—this imparts an isotopically-heavy Ba  
464 signal at the depths where the influence from ULSW is greatest.

465 These subtle features in the depth profile that are largely undetectable from examination of

466 [Ba] illustrate that Ba isotope distributions are highly sensitive to ocean circulation, highlighting the  
467 possible utility of Ba isotopes as a powerful tracer of basin-scale hydrography in paleoceanographic  
468 studies.

469

#### 470 *4.3.3. The sediment-water interface: a sedimentary source for dissolved Ba?*

471 The limited number of near-bottom water samples collected from the tropical North  
472 Atlantic, in particular the eastern basin, show a slight deviation towards heavier  $\delta^{138}\text{Ba}$  at the very  
473 base of the profile (Fig. 3). We have no reason to believe that these signals are an analytical artefact  
474 or a blank issue for two reasons. Firstly, these samples were not atypical in other respects (e.g. T, S,  
475  $[\text{O}_2]$ ), suggesting that the bottles fired at the correct depths. Secondly, the Ba-isotopic composition  
476 of the procedural Ba blank was measured as  $\approx 0\text{‰}$  (Horner et al., 2015), whereas these bottom  
477 water samples exhibit shifts toward isotopically heavy Ba of  $\approx +0.4\text{‰}$  rather than towards the  
478 isotopic composition of the blank. Our results hint towards a sedimentary source of dissolved Ba into  
479 these bottom waters since dissolved [Ba] and  $\text{Ba}^*$  show significant upticks at the very base of the  
480 profile, whereas a water mass signal would presumably also affect [Si] or other hydrographic  
481 parameters. The direction of the  $\delta^{138}\text{Ba}$  anomaly is opposite of that expected if the signature was a  
482 result of sinking barite, which would be expected to add Ba with an isotopic composition  $\approx +0.3\text{‰}$   
483 (assuming  $\text{BaSO}_4$  precipitates are  $\approx -0.2$  to  $-0.4\text{‰}$  lighter than mesopelagic waters; e.g. Von Allmen  
484 et al., 2010; Horner et al., 2015; Cao et al., 2016). Instead, this Ba may be sourced from seafloor  
485 sediments, which would indicate possible Ba-isotopic fractionation effects during sediment  
486 diagenesis. Significant diffusive efflux of Ba from sediments under sulphate-reducing conditions has  
487 been previously noted (Hoppema et al., 2010; McManus et al., 1994), and could provide a possible  
488 mechanism for the apparent injection of isotopically 'heavy' Ba into overlying seawaters with lighter  
489 compositions. However, recent laboratory experiments (van Zuilen et al., 2016) have shown that  
490 diffusive transport results in a preferential release of isotopically light Ba, and that adsorption  
491 preferentially retains isotopically heavy Ba—both of these effects have the opposite fractionation  
492 factor to the patterns observed here. Clearly, further work into the nature of this isotopic  
493 enrichment is justified, including further field-based studies, given that sediments are a potentially  
494 important source of dissolved Ba to abyssal depths.

495

#### 496 *4.4. Synthesis: Decoupling of barium concentrations and isotopic composition in the Atlantic*

497

##### 498 *4.4.1. A conceptual model for Ba cycling in the Atlantic*

499 One of the key observations in our new data is that there is a stronger meridional variation



500 in Ba concentrations compared to  $\delta^{138}\text{Ba}$  (Fig. 3). This apparent decoupling may be as a result of a  
501 low fractionation of Ba during barite formation, resulting in relatively subtle variations in  $\delta^{138}\text{Ba}$  and  
502 a larger dissolved pool relative to particulate phases (Dehairs et al., 1991). Despite the overprint of  
503 barite remineralisation, Ba and  $\delta^{138}\text{Ba}$  variations can be traced along the meridional ocean  
504 circulation resulting in a conceptual model (Fig. 7) of the Ba cycle that is consistent with our new  
505 observations.

506 A greater concentration of Ba in southern sourced mode waters in the tropics compared to  
507 40°S is consistent with a gradual stripping of Ba in the upper mesopelagic layer (200-400m) as a  
508 result of barite formation as the water mass is transported north by meridional circulation. Barite  
509 formation results in a small fractionation of Ba isotopes, resulting in the insignificant difference in  
510  $\delta^{138}\text{Ba}$  between mode waters in the near-surface waters of the tropics compared to the South  
511 Atlantic, despite having undergone extensive Ba removal into  $\text{BaSO}_4$  formation. In addition, there is  
512 also a re-entrainment of deeper water in the Equatorial upwelling regions, potentially allowing a  
513 certain degree of resetting on Ba-isotopic values. The rapid transit of water via LSW will also mean  
514 that samples in the mid-depths of the western basin will have heavier Ba-isotopes and lower [Ba]  
515 than waters from the corresponding isopycnal in the eastern basin centred at approximately 1500m.  
516 Similarly, NADW at 40°S has a greater Ba concentration than in the North Atlantic as a result of  
517 “ageing” (barite dissolution, with a small contribution from the remineralisation of other Ba-bearing  
518 minerals e.g. celestite ) along the meridional ocean circulation path and more AABW entrainment at  
519 depth.

520

#### 521 *4.4.2 Implications for the use of Ba-based proxies in palaeoceanography*

522 Our [Ba] and  $\delta^{138}\text{Ba}$  depth profiles provide useful insights into the utility of carbonate Ba/Ca  
523 as geochemical archives of ocean conditions. Firstly, the  $\delta^{138}\text{Ba}$  data from the North Atlantic are  
524 consistent with the formation of barite in subsurface waters, below 150 m, at the top of the  
525 mesopelagic layer rather than deeper in the water column, supporting the paradigm that barite  
526 formation occurs at similar depths associated with organic carbon remineralization and export.  
527 Secondly, our data support the recently advanced hypothesis that variations in the relationship  
528 between [Ba],  $\delta^{138}\text{Ba}$  and dissolved [Si] are largely driven by ocean circulation and are set by the  
529 degree of barite formation in the subsurface waters of the high latitudes – where intermediate and  
530 deep waters are ventilated and subducted into the ocean interior (Horner et al., 2015). Small  
531 variations in the relationship between [Ba] and [Si]—quantified here using  $\text{Ba}^*$ —point to Ba-specific  
532 overprinting through barite cycling, which imparts minor changes to Ba distributions but does not  
533 affect Si. However, these changes in Ba cycling are small relative to the overall structure of dissolved

534 [Ba] and [Si] profiles, which are set by large-scale circulation processes. These observations suggest  
535 that geochemical archives of [Ba], such as foraminiferal Ba/Ca, coupled together with proxies for  
536 marine silicon cycling, could shed light on changes in high latitude carbon export and recycling.  
537 Moreover, reconstruction of deep ocean Ba isotopes could provide insight into the advective origin  
538 of water masses in the deep ocean and thus the geometry of the MOC through time, subject to the  
539 identification of appropriate sedimentary archives.

540

## 541 **5. Conclusion**

542

543 We present four new full barium isotope depth profiles from the North and South Atlantic  
544 Ocean, allowing a robust assessment of both zonal and meridional Ba cycling across the Atlantic. Our  
545 data show that sub-surface barite formation results in heavy seawater  $\delta^{138}\text{Ba}$  at approximately 200-  
546 400m depth, at the top of the mesopelagic layer, and that mesopelagic Ba-isotopic heterogeneity is  
547 likely determined by the depth of the mixed layer relative to that of barite formation. Below the  
548 depths of barite formation, Ba and  $\delta^{138}\text{Ba}$  systematics are mostly controlled by large-scale ocean  
549 circulation (i.e. conservative Ba cycling), with a subtle overprint from regenerated Ba that we  
550 attribute to *in situ* barite dissolution. We synthesize these findings to present a conceptual model of  
551 barium systematics in the Atlantic, which indicates that deep-water barium concentrations and  
552 isotopic variations can be explained by conservative mixing between NADW and AABW with  $\delta^{138}\text{Ba}$   
553 of the two end-members determined as +0.45 and +0.26 ‰, respectively. This mixing model  
554 suggests that Ba isotopes may facilitate tracing the proportion of northern- versus southern-sourced  
555 waters filling the deep Atlantic in the geological past—and therefore the geometry of deep ocean  
556 circulation—from a single biogeochemical tracer. These results underscore the importance of large-  
557 scale mixing as the proximal cause of the strong correlation between dissolved [Ba] and [silicate] in  
558 the Atlantic, thereby highlighting the utility of barium isotopes to understand the processes  
559 governing marine Ba cycling. Application of Ba isotopes to marine chemistry thus harbours great  
560 promise as a new means to probe the mechanisms governing Ba-based tracers in paleoceanography,  
561 and how these relate to the temporal evolution of the oceans biological carbon pump.

562

563

## 564 **Acknowledgements**

565 The authors would like to thank the captain and crew of the RRS James Cook and the RRS Discovery,  
566 and all who took part in JC094 and GA10E/D357. Thanks to Paul Morris for bottle oxygen  
567 concentration measurements on JC094, Clark Richards for CTD data processing, and Sune Nielsen for

568 discussions. D357/GA10E was funded by the UK-GEOTRACES National Environment Research Council  
569 Consortium Grant (NE/H006095/1) and JC094 by the European Research Council. KH thanks The  
570 Royal Society (University Research Fellowship UF120084) and FP7-PEOPLE-2012-CIG Proposal No  
571 320070 for funding; TJH thanks The Andrew W. Mellon Foundation Endowed Fund for Innovative  
572 Research, NSF (OCE-1443577), and the Agouron Institute Geobiology Postdoctoral Fellowship  
573 Program for supporting isotope research at NIRVANA. The authors express sincere thanks to the  
574 three anonymous reviewers who helped us to substantially improve the manuscript with their  
575 constructive comments.

576

### 577 **Figure captions**

578

579 Figure 1: Map showing locations of seawater profiles: CTD002, CTD005 and CTD006 (stations  
580 2, 39 and 49, respectively) from cruise JC094; CTD013 and CTD025 (stations 3 and 6 from cruise  
581 D357/GA10E); CTD025 data from Horner et al., 2015. Colour contours show maximum mixed layer  
582 depths (calculated from the monthly means) from National Oceanographic and Atmospheric  
583 Administration Monthly Isopycnal & Mixed-layer Ocean Climatology (Schmidtko et al., 2013).  
584 Produced using Ocean Data View (Schlitzer, 2000).

585

586 Figure 2: Water properties at the CTD stations used in this study: A) Potential temperature;  
587 B) Salinity; C) Oxygen; D) Nitrate; E) Si\*; and F) Si(OH)<sub>4</sub> concentration. The figure legends apply to all  
588 subsequent figures.

589

590 Figure 3: A) Barium concentrations and B) Barium isotopic compositions of the seawater  
591 samples analysed in this study. Equatorial Atlantic data are plotted in red (Eastern Equatorial) and  
592 blue (Western Equatorial) with circle symbols, South Eastern Atlantic data are plotted in black with  
593 triangle symbols. Open triangle symbols and black dashed curves show previously-published data  
594 from the South East Atlantic at 40°S (Horner et al., 2015). Error bar shows representative  $\pm 2SD$   
595 ( $\pm 0.035\%$ ). The uncertainties on the barium concentration are within the size of the symbols. See  
596 Figure 2 for legend.

597

598 Figure 4: Ba\* plotted against depth and barium isotopic composition for seawater for A) the  
599 Eastern Equatorial Atlantic (red) and Western Equatorial Atlantic (blue) and B) the South East  
600 Atlantic, including previously-published data from the South East Atlantic at 40°S (open triangle

601 symbols and black dashed curves; Horner et al., 2015). See main text for details on how Ba\* is  
602 calculated. Error bar shows representative  $\pm 2SD$  ( $\pm 0.035\%$ ). See Figure 2 for legend.

603

604 Figure 5: Plots of A) fluorescence, B) oxygen concentration, C) Ba\* and D)  $\delta^{138}\text{Ba}$  in the top  
605 1000m at the different study sites. Tropical Atlantic data are plotted in red (Eastern Equatorial) and  
606 blue (Western Equatorial) with circle symbols, South Eastern Atlantic data are plotted in black with  
607 triangle symbols. Open triangle symbols and black dashed curves show previously-published data  
608 from the South East Atlantic at 40°S (Horner et al., 2015) (see Figure 2 for legend). Error bar shows  
609 representative  $\pm 2SD$  ( $\pm 0.035\%$ ).

610

611 Figure 6: A) Mixing lines of  $\delta^{138}\text{Ba}$  plotted against  $1/\text{Ba}$  for the seawater samples from the  
612 tropical North Atlantic (circles) and the South Atlantic at approximately 40°S (triangles; Horner et al.,  
613 2015). Error bars show representative  $\pm 2SD$  ( $\pm 0.035\%$ ). Least-squares linear regression lines are  
614 plotted separately for the tropical North Atlantic (solid line;  $r^2 = 0.73$ ,  $p < 0.05$ ) and South East  
615 Atlantic (dashed line;  $r^2 = 0.93$ ,  $p < 0.05$ ) using data from  $\geq 500\text{m}$ . Grey symbols show samples from  
616 shallower than 500m, which were not included in the regression calculation. B) Calculated best-fit  
617 mixing line between northern- and southern-sourced water masses in the Atlantic below 2,000 m  
618 (see text for calculation details). The excellent agreement between the simple mixing relationship  
619 and our seawater data suggest that it is possible to independently estimate  $f_n$  from Ba isotope  
620 analyses using the relationship:  $f_n \approx [ 21 (50 \delta^{138/134}\text{Ba}_{\text{NIST}} - 13) ] / (550 \delta^{138/134}\text{Ba}_{\text{NIST}} - 48)$ , which is  
621 valid over the range of  $\delta^{138/134}\text{Ba}_{\text{NIST}} = +0.26$  to  $+0.45 \%$ ; predictive error = 13 %.

622

623 Figure 7: Conceptual model of Ba cycling in the Atlantic. Southern component waters are  
624 enriched in Ba relative to Si. Southern sourced intermediate/mode waters (i.e. AAIW) are gradually  
625 stripped of Ba as a result of barite formation and mixing as the water mass moves north, reducing  
626 Ba\* but having minimal impact on  $\delta^{138}\text{Ba}$ . NADW/CDW at 40°S has a greater Ba concentration than  
627 in the North Atlantic as a result of barite dissolution and AABW entrainment during water mass  
628 ageing. (Figure design by Jack Cook, Woods Hole Oceanographic Institution.)

629

630

631

## 632 References

633 Bertram, M.A., Cowen, J.P., 1997. Morphological and compositional evidence for biotic precipitation  
634 of marine barite. *Journal of Marine Research* 55, 577-593.

635 Bishop, J., 1989. Regional extremes in particulate matter composition and flux: effects on the  
636 chemistry of the ocean interior. *Productivity of the ocean: present and past* 44, 117-137.

637 Böttcher, M.E., Geprägs, P., Neubert, N., Von Allmen, K., Pretet, C., Samankassou, E., Nägler, T.F.,  
638 2012. Barium isotope fractionation during experimental formation of the double carbonate BaMn  
639 [CO<sub>3</sub>]<sub>2</sub> at ambient temperature. *Isotopes in environmental and health studies* 48, 457-463.

640 Brewer, P., Riley, J., 1965. The automatic determination of nitrate in sea water, *Deep Sea Research*  
641 and *Oceanographic Abstracts*. Elsevier, pp. 765-772.

642 Broecker, W.S., Peng, T.-H., 1982. *Tracers in the Sea*. Eldigio Press.

643 Broecker, W.S., Takahashi, T., Takahashi, T., 1985. Sources and flow patterns of deep-ocean waters  
644 as deduced from potential temperature, salinity, and initial phosphate concentration. *Journal of*  
645 *Geophysical Research: Oceans* 90, 6925-6939.

646 Brzezinski, M.A., Sigman, D.M., Sarmiento, J.L., Matsumoto, K., Gruber, N., Rau, G.H., Coale, K.H.,  
647 2002. A switch from Si(OH)<sub>4</sub> to NO<sub>3</sub><sup>-</sup> depletion in the glacial Southern Ocean. *Geophysical Research*  
648 *Letters* 29, 1564.

649 Cao, Z., Siebert, C., Hathorne, E.C., Dai, M., Frank, M., 2016. Constraining the oceanic barium cycle  
650 with stable barium isotopes. *Earth and Planetary Science Letters* 434, 1-9.

651 Cardinal, D., Savoye, N., Trull, T.W., André, L., Kopczynska, E.E., Dehairs, F., 2005. Variations of  
652 carbon remineralisation in the Southern Ocean illustrated by the Ba xs proxy. *Deep Sea Research*  
653 *Part I: Oceanographic Research Papers* 52, 355-370.

654 Carritt, D.E., Carpenete, J., 1966. Comparison and evaluation of currently employed modifications of  
655 Winkler method for determining dissolved oxygen in seawater-a NASCO Report. *Journal of Marine*  
656 *Research* 24, 286-&.

657 Chen, T., Robinson, L.F., Burke, A., Southon, J., Spooner, P., Morris, P.J., Ng, H.C., 2015. Synchronous  
658 centennial abrupt events in the ocean and atmosphere during the last deglaciation. *Science* 349,  
659 1537-1541.

660 Collier, R., Edmond, J., 1984. The trace element geochemistry of marine biogenic particulate matter.  
661 *Progress in Oceanography* 13, 113-199.

662 Craig, H., Turekian, K., 1980. The GEOSECS program: 1976–1979. *Earth and Planetary Science Letters*  
663 49, 263-265.

664 Cutter, G., Andersson, P., Codispoti, L., Croot, P., Francois, R., Lohan, M., Obata, H., Rutgers vd Loeff,  
665 M., 2010. Sampling and sample-handling protocols for GEOTRACES Cruises.

666 Dehairs, F., Chesselet, R., Jedwab, J., 1980. Discrete suspended particles of barite and the barium  
667 cycle in the open ocean. *Earth and Planetary Science Letters* 49, 528-550.

668 Dehairs, F., Jacquet, S., Savoye, N., Van Mooy, B.A., Buesseler, K.O., Bishop, J.K., Lamborg, C.H.,  
669 Elskens, M., Baeyens, W., Boyd, P.W., 2008. Barium in twilight zone suspended matter as a potential  
670 proxy for particulate organic carbon remineralization: Results for the North Pacific. *Deep Sea*  
671 *Research Part II: Topical Studies in Oceanography* 55, 1673-1683.

672 Dehairs, F., Stroobants, N., Goeyens, L., 1991. Suspended barite as a tracer of biological activity in  
673 the Southern Ocean. *Marine Chemistry* 35, 399-410.

674 Dymond, J., Suess, E., Lyle, M., 1992. Barium in deep-sea sediment: A geochemical indicator of  
675 paleoproductivity. *Paleoceanography* 7, 163-181.

676 Eagle, M., Paytan, A., Arrigo, K.R., van Dijken, G.L., Murray, R.W., 2003. A comparison between  
677 excess barium and barite as indicators of carbon export. *Paleoceanography* 18, Art. no. 1021.

678 Foster, D.A., Staubwasser, M., Henderson, G.M., 2004. 226 Ra and Ba concentrations in the Ross Sea  
679 measured with multicollector ICP mass spectrometry. *Marine chemistry* 87, 59-71.

680 Ganeshram, R.S., Francois, R., Commeau, J., Brown-Leger, S.L., 2003. An experimental investigation  
681 of barite formation in seawater. *Geochimica et Cosmochimica Acta* 67, 2599-2605.

682 Gingele, F., Dahmke, A., 1994. Discrete barite particles and barium as tracers of paleoproductivity in  
683 South Atlantic sediments. *Paleoceanography* 9, 151-168.

684 González-Munoz, M.T., Fernández-Luque, B., Martínez-Ruiz, F., Chekroun, K.B., Arias, J.M.,  
685 Rodríguez-Gallego, M., Martínez-Canamero, M., De Linares, C., Paytan, A., 2003. Precipitation of

686 barite by *Myxococcus xanthus*: possible implications for the biogeochemical cycle of barium. *Applied*  
687 *and Environmental Microbiology* 69, 5722-5725.

688 Grasshoff, K., Kremling, K., Ehrhardt, M., 1999. *Methods of seawater analysis*. John Wiley & Sons.

689 Griffith, E.M., Paytan, A., 2012. Barite in the ocean—occurrence, geochemistry and  
690 palaeoceanographic applications. *Sedimentology* 59, 1817-1835.

691 Gruber, N., Sarmiento, J.L., 1997. Global patterns of marine nitrogen fixation and denitrification  
692 *Global Biogeochemical Cycles* 11, 235-366.

693 Hall, J.M., Chan, L.-H., 2004a. Ba/Ca in benthic foraminifera: thermocline and middepth circulation in  
694 the North Atlantic during the last glaciation. *Paleoceanography* 19, Art. no. PA4018.

695 Hall, J.M., Chan, L.-H., 2004b. Ba/Ca in *Neogloboquadrina pachyderma* as an indicator of deglacial  
696 meltwater discharge into the western Arctic Ocean. *Paleoceanography* 19,  
697 doi:10.1029/2003PA000910.

698 Hernandez-Sanchez, M.T., Mills, R.A., Planquette, H., Pancost, R.D., Hepburn, L., Salter, I.,  
699 FitzGeorge-Balfour, T., 2011. Quantifying export production in the Southern Ocean: Implications for  
700 the Baxs proxy. *Paleoceanography* 26.

701 Hoefs, J., 2015. Isotope fractionation processes of selected elements, *Stable Isotope Geochemistry*.  
702 Springer, pp. 47-190.

703 Hoppema, M., Dehairs, F., Navez, J., Monnin, C., Jeandel, C., Fahrbach, E., De Baar, H., 2010.  
704 Distribution of barium in the Weddell Gyre: Impact of circulation and biogeochemical processes.  
705 *Marine Chemistry* 122, 118-129.

706 Horner, T.J., Kinsley, C.W., Nielsen, S.G., 2015. Barium-isotopic fractionation in seawater mediated  
707 by barite cycling and oceanic circulation. *Earth and Planetary Science Letters* 430, 511-522.

708 Jacquet, S., Dehairs, F., Elskens, M., Savoye, N., Cardinal, D., 2007. Barium cycling along WOCE SR3  
709 line in the Southern Ocean. *Marine Chemistry* 106, 33-45.

710 Jacquet, S., Dehairs, F., Savoye, N., Obernosterer, I., Christaki, U., Monnin, C., Cardinal, D., 2008.  
711 Mesopelagic organic carbon remineralization in the Kerguelen Plateau region tracked by biogenic  
712 particulate Ba. *Deep Sea Research Part II: Topical Studies in Oceanography* 55, 868-879.

713 Jenkins, W., Smethie, W., Boyle, E., Cutter, G., 2015. Water mass analysis for the US GEOTRACES  
714 (GA03) North Atlantic sections. *Deep Sea Research Part II: Topical Studies in Oceanography* 116, 6-  
715 20.

716 Kara, A.B., Rochford, P.A., Hurlburt, H.E., 2003. Mixed layer depth variability over the global ocean.  
717 *Journal of Geophysical Research: Oceans* 108.

718 Kirkwood, D., 1989. Simultaneous determination of selected nutrients in sea water. *International*  
719 *Council for the Exploration of the Sea (ICES) CM* 100, 29.

720 Lea, D.W., Boyle, E.A., 1989. Barium content of benthic foraminifera controlled by bottom-water  
721 composition. *Nature* 338, 751-753.

722 Lea, D.W., Boyle, E.A., 1991. Barium in planktonic foraminifera. *Geochimica Cosmochimica Acta* 55,  
723 3321-3331.

724 McManus, J., Berelson, W.M., Klinkhammer, G.P., Kilgore, T.E., Hammond, D.E., 1994. Remobilization  
725 of barium in continental margin sediments. *Geochimica et Cosmochimica Acta* 58, 4899-4907.

726 Miyazaki, T., Kimura, J.-I., Chang, Q., 2014. Analysis of stable isotope ratios of Ba by double-spike  
727 standard-sample bracketing using multiple-collector inductively coupled plasma mass spectrometry.  
728 *Journal of Analytical Atomic Spectrometry* 29, 483-490.

729 Monnin, C., Jeandel, C., Cattaldo, T., Dehairs, F., 1999. The marine barite saturation state of the  
730 world's oceans. *Marine Chemistry* 65, 253-261.

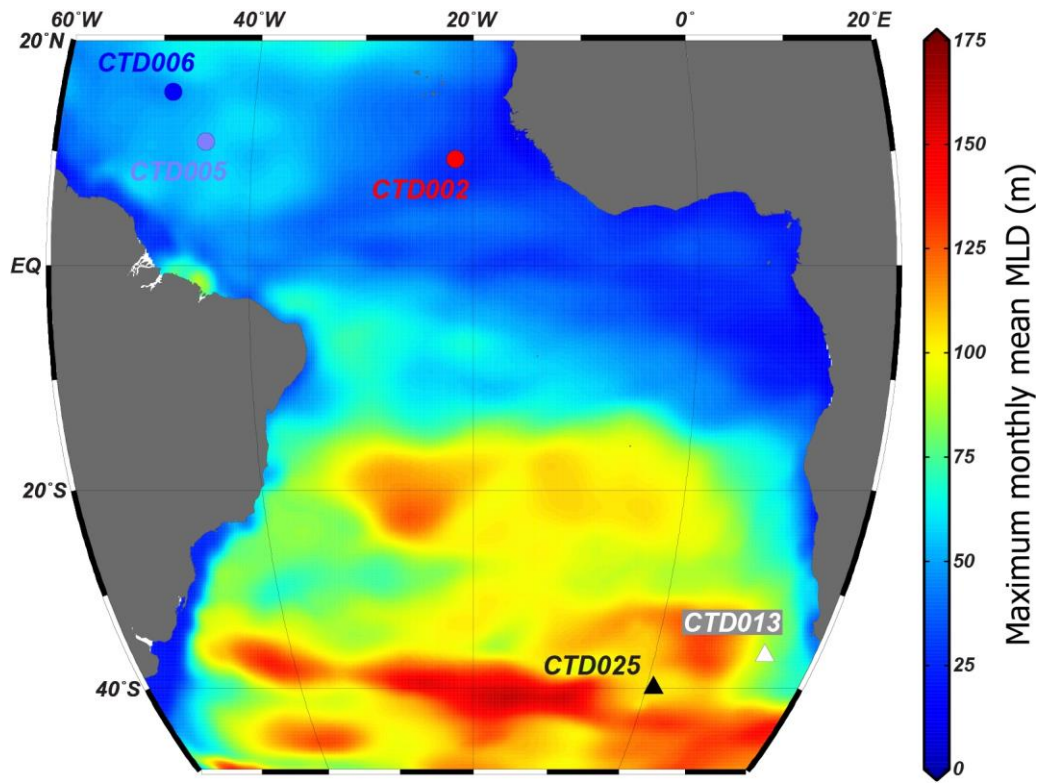
731 Nan, X., Wu, F., Zhang, Z., Hou, Z., Huang, F., Yu, H., 2015. High-precision barium isotope  
732 measurements by MC-ICP-MS. *Journal of Analytical Atomic Spectrometry* 30, 2307-2315.

733 Nelson, D.M., Treguer, P., Brzezinski, M.A., Leynaert, A., Queguiner, B., 1995. Production and  
734 dissolution of biogenic silica in the ocean: revised global estimates, comparison with regional data  
735 and relationship to biogenic sedimentation. *Global Biogeochemical Cycles* 9, 359-372.

736 Nurnberg, C.C., Bohrmann, G., Schluter, M., Frank, M., 1997. Barium accumulation in the Atlantic  
737 sector of the Southern Ocean: results from 19,000 year records. *Paleoceanography* 12, 594-603.  
738 Paytan, A., Kastner, M., 1996. Benthic Ba fluxes in the central Equatorial Pacific, implications for the  
739 oceanic Ba cycle. *Earth and Planetary Science Letters* 142, 439-450.  
740 Riebesell, U., Schulz, K.G., Bellerby, R., Botros, M., Fritsche, P., Meyerhöfer, M., Neill, C., Nondal, G.,  
741 Oschlies, A., Wohlers, J., 2007. Enhanced biological carbon consumption in a high CO<sub>2</sub> ocean. *Nature*  
742 450, 545-548.  
743 Robinson, L.F., 2014. RRS James Cook Cruise JC094, October 13–November 30 2013, Tenerife-  
744 Trinidad. TROPICS, Tracing Oceanic Processes using Corals and Sediments. Reconstructing abrupt  
745 Changes in Chemistry and Circulation of the Equatorial Atlantic Ocean: Implications for global  
746 Climate and deep-water Habitats.  
747 Sarmiento, J.L., Gruber, N., Brzezinski, M.A., Dunne, J.P., 2004. High-latitude controls of thermocline  
748 nutrients and low latitude biological productivity. *Nature* 427, 56-60.  
749 Schlitzer, R., 2000. Electronic atlas of WOCE hydrographic and tracer data now available. *EOS Trans.*  
750 AUG 81, 45.  
751 Schmidtko, S., Johnson, G.C., Lyman, J.M., 2013. MIMOC: A global monthly isopycnal upper-ocean  
752 climatology with mixed layers. *Journal of Geophysical Research: Oceans* 118, 1658-1672.  
753 Sternberg, E., Tang, D., Ho, T.-Y., Jeandel, C., Morel, F.M., 2005. Barium uptake and adsorption in  
754 diatoms. *Geochimica et Cosmochimica Acta* 69, 2745-2752.  
755 Talley, L.D., 2013. Closure of the global overturning circulation through the Indian, Pacific, and  
756 Southern Oceans: Schematics and transports. *Oceanography* 26, 80-97.  
757 Talley, L.D., Pickard, G.L., Emery, W.J., Swift, J.H., 2011. *Descriptive physical oceanography: an*  
758 *introduction*. Academic Press.  
759 Tilstone, G.H., Taylor, B.H., Blondeau-Patissier, D., Powell, T., Groom, S.B., Rees, A.P., Lucas, M.I.,  
760 2015. Comparison of new and primary production models using SeaWiFS data in contrasting  
761 hydrographic zones of the northern North Atlantic. *Remote Sensing of Environment* 156, 473-489.  
762 Tréguer, P., De la Rocha, C.L., 2013. The world ocean silica cycle. *Annual Review of Marine Science* 5,  
763 477-501.  
764 van Zuilen, K., Müller, T., Nägler, T.F., Dietzel, M., Küsters, T., 2016. Experimental determination of  
765 barium isotope fractionation during diffusion and adsorption processes at low temperatures.  
766 *Geochimica et Cosmochimica Acta* In press.  
767 Varela, D.E., Pride, C.J., Brzezinski, M.A., 2004. Biological fractionation of silicon isotopes in Southern  
768 Ocean surface waters. *Global Biogeochemical Cycles* 18, doi:10.1029/2003GB002140.  
769 Von Allmen, K., Böttcher, M.E., Samankassou, E., Nägler, T.F., 2010. Barium isotope fractionation in  
770 the global barium cycle: First evidence from barium minerals and precipitation experiments.  
771 *Chemical Geology* 277, 70-77.  
772 Zhang, J.-Z., Chi, J., 2002. Automated analysis of nanomolar concentrations of phosphate in natural  
773 waters with liquid waveguide. *Environmental science & technology* 36, 1048-1053.

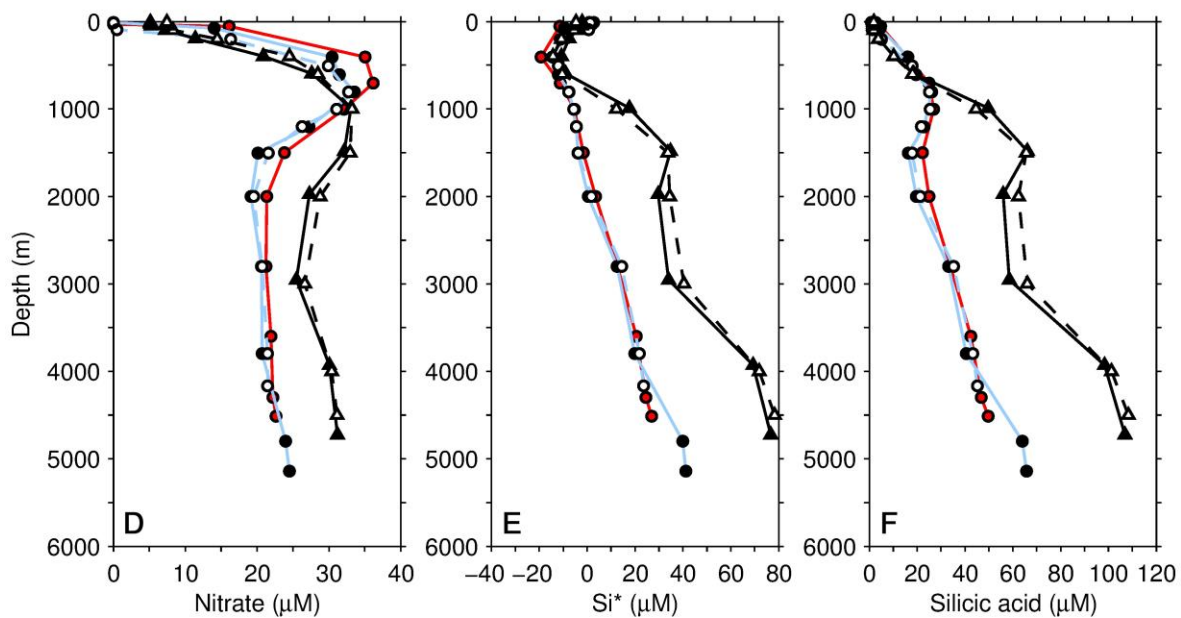
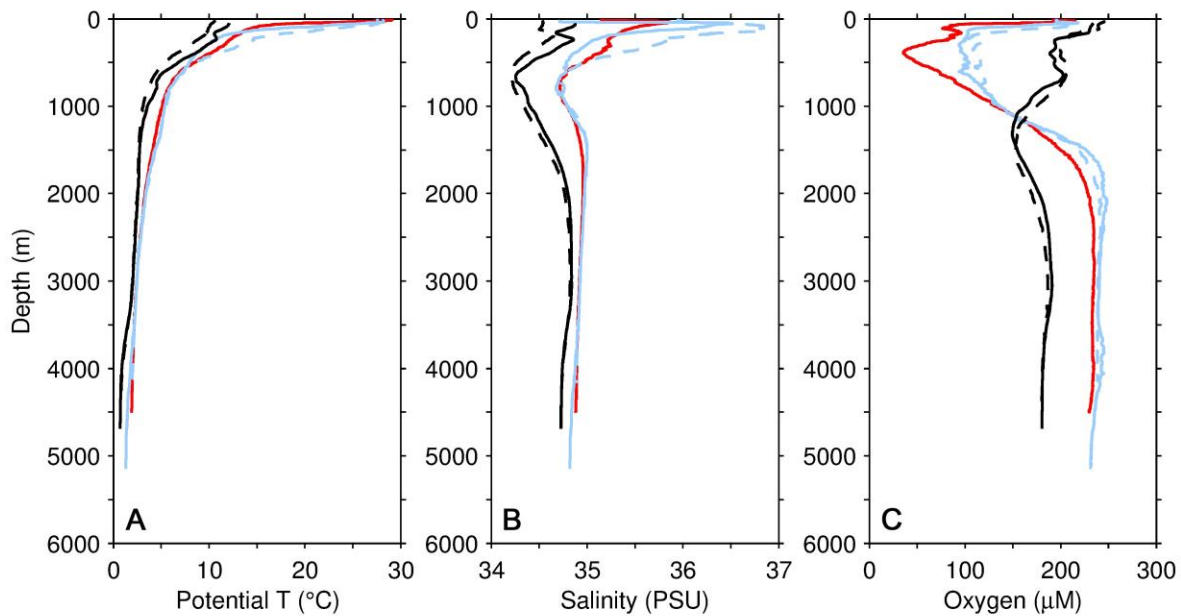
774

775



776





**Sensor data (A, B, C)**

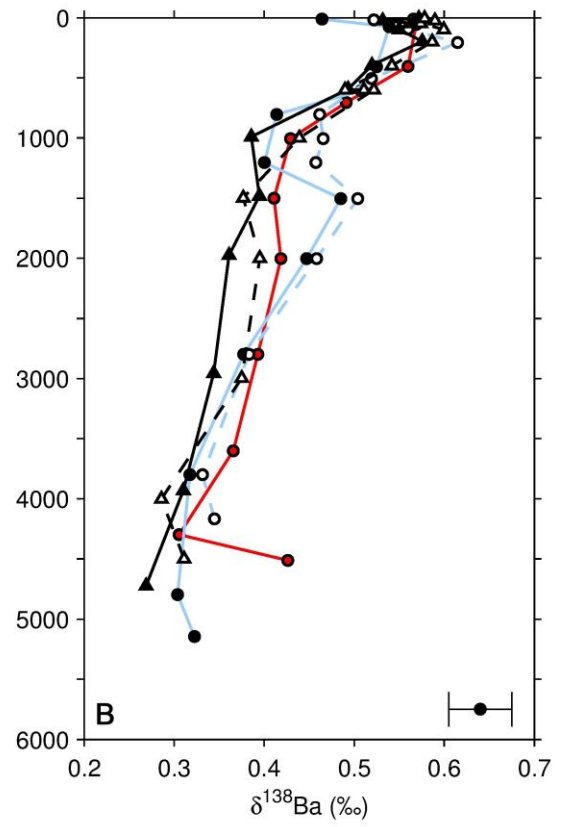
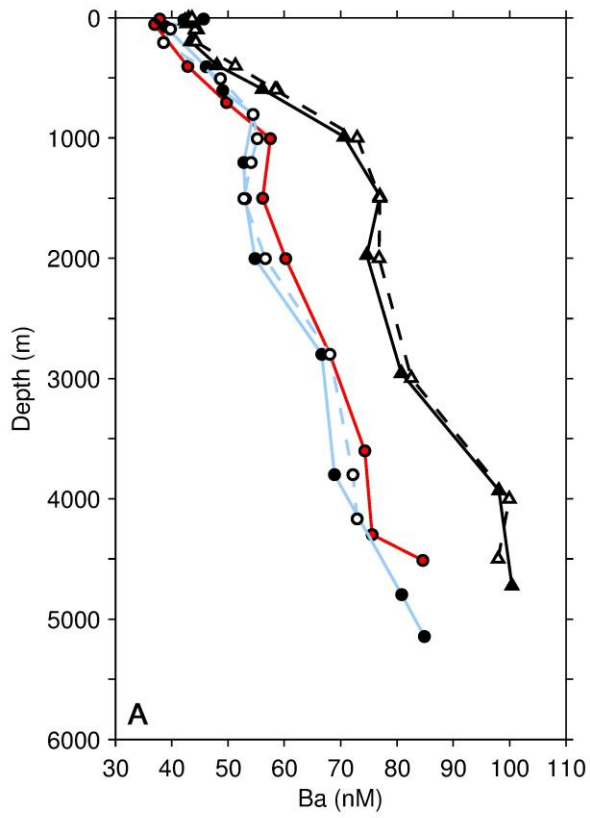
- NE (JC094 CTD2)
- NW (JC094 CTD5)
- - NW (JC094 CTD6)
- SE (D357 CTD13)
- - SE (D357 CTD25) (Horner et al., 2015)

**Bottle data (D, E, F)**

- NE (JC094 CTD2)
- NW (JC094 CTD5)
- NW (JC094 CTD6)
- ▲ SE (D357 CTD13)
- ▲ SE (D357 CTD25) (Horner et al., 2015)

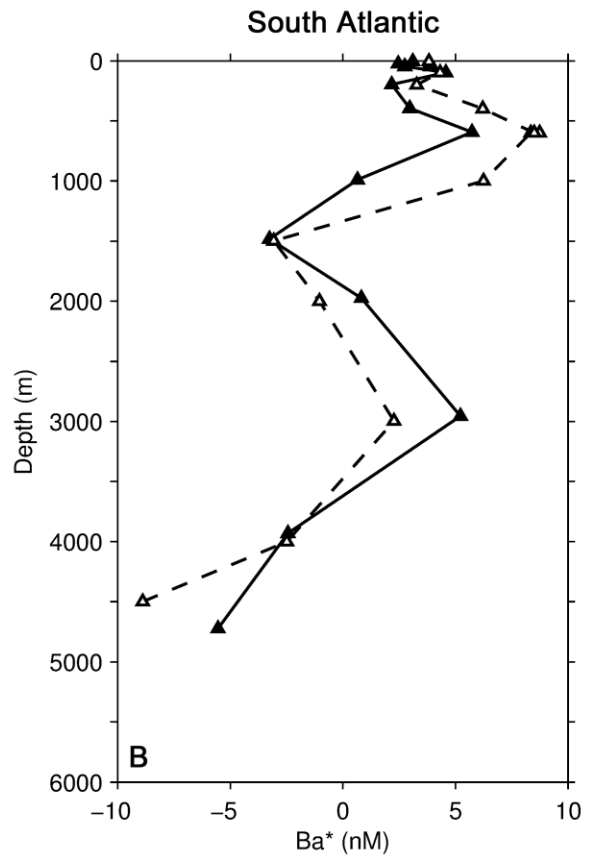
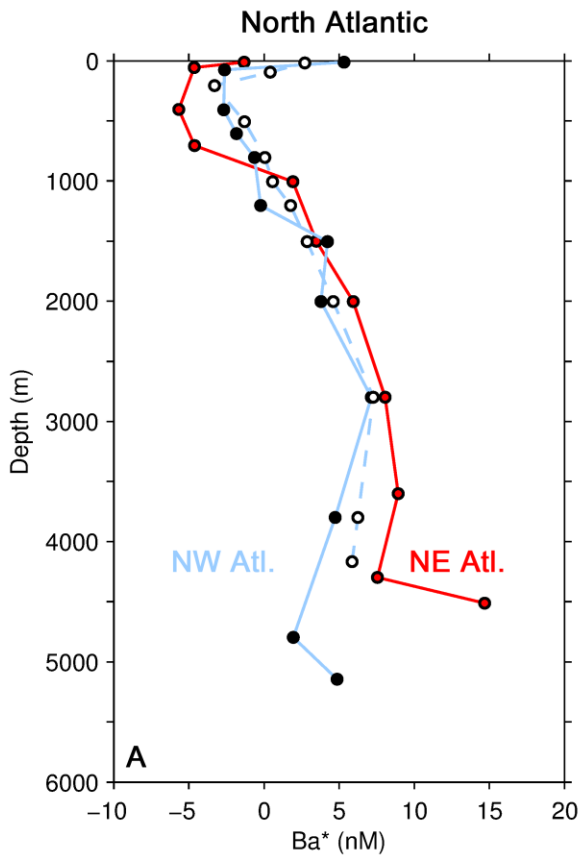
777

778



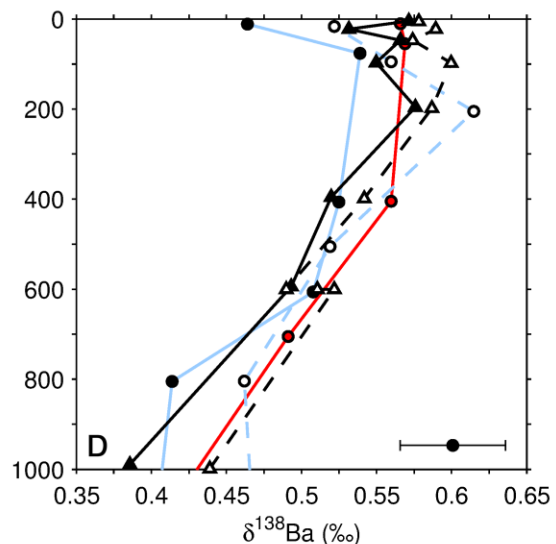
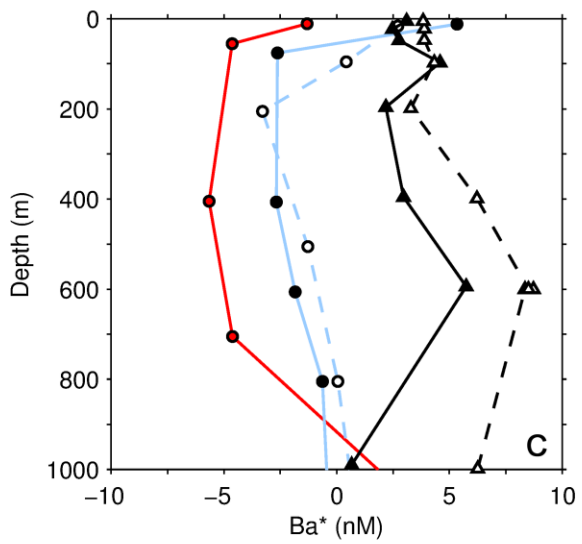
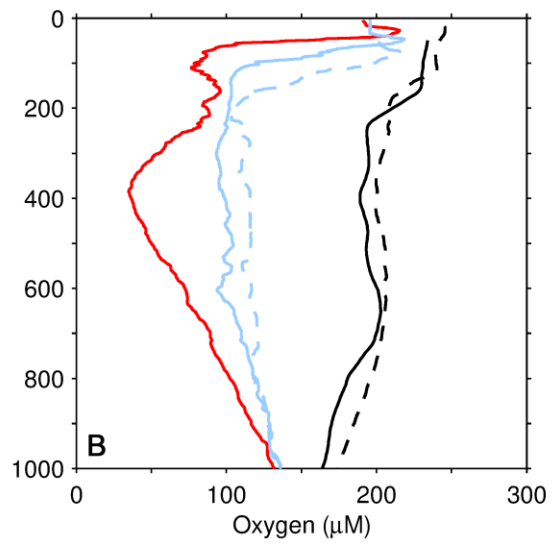
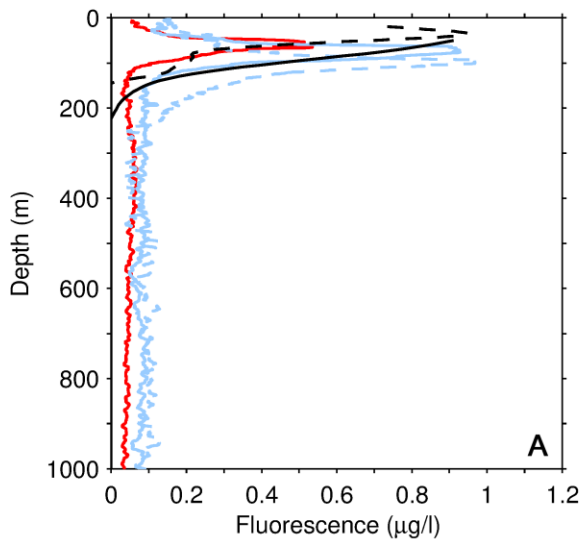
779

780



781

782



**Sensor data (A, B)**

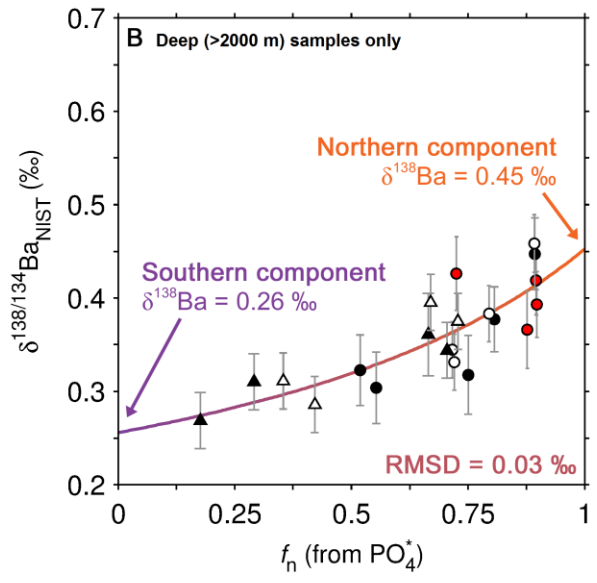
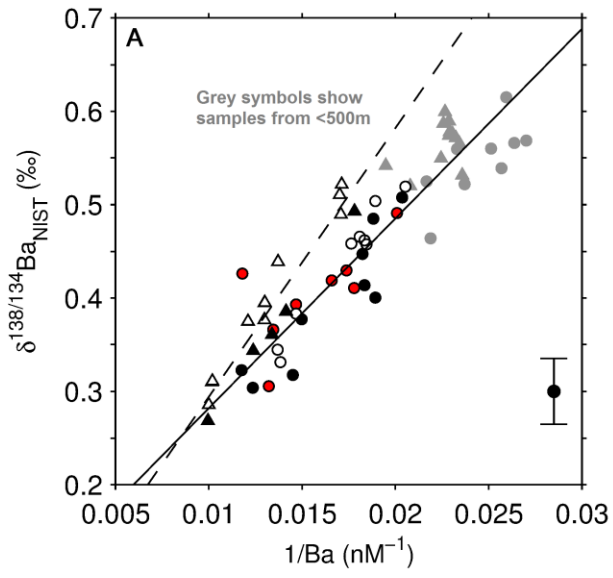
- NE (JC094 CTD2)
- NW (JC094 CTD5)
- - - NW (JC094 CTD6)
- SE (D357 CTD13)
- - - SE (D357 CTD25) (Horner et al., 2015)

**Bottle data (C, D)**

- NE (JC094 CTD2)
- NW (JC094 CTD5)
- NW (JC094 CTD6)
- ▲ SE (D357 CTD13)
- ▲ SE (D357 CTD25) (Horner et al., 2015)

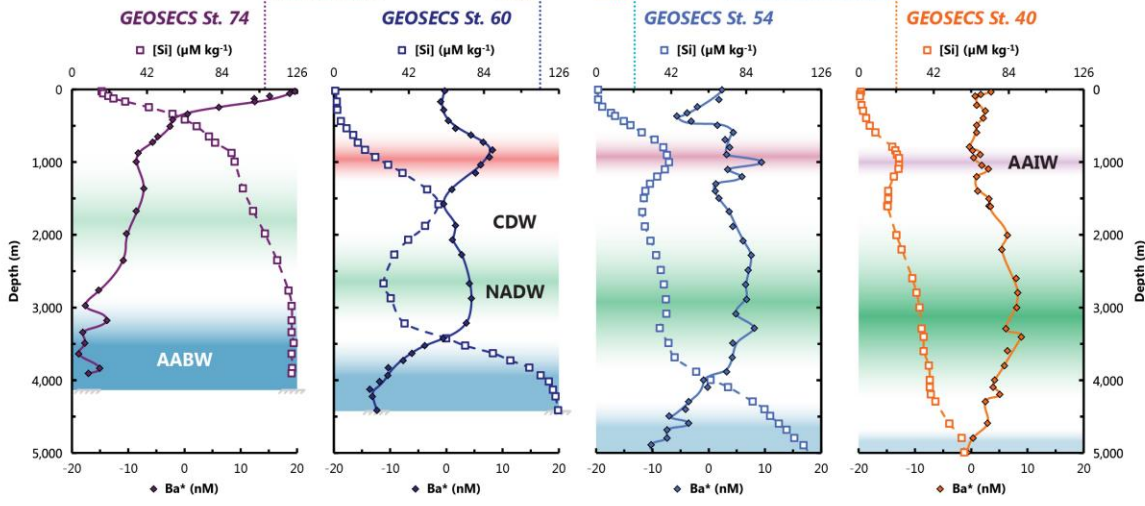
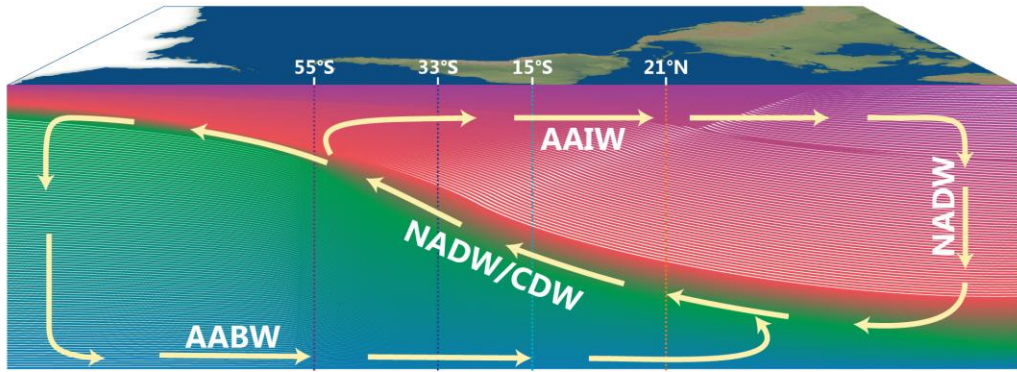
783

784



785

786



787